Applied Physics B (2021) 127:9
https://doi.org/10.1007/s00340-020-07561-x

Applied Physics B
Lasers and Optics

Potassium L-ascorbate monohydrate: a new metal–organic nonlinear optical crystal

Dhanpal Bairwa[1] · K. Raghavendra Rao[2] · Diptikanta Swain[3] · Tayur N. Guru Row[3] · H. L. Bhat[1] · Suja Elizabeth[1]

Received: 14 September 2019 / Accepted: 30 November 2020 / Published online: 6 January 2021
© The Author(s), under exclusive licence to Springer-Verlag GmbH, DE part of Springer Nature 2021

Abstract

Large size single crystals of potassium L-ascorbate monohydrate, $KC_6H_7O_6.H_2O$ (KLAM), are grown using solution growth technique by lowering the temperature at the rate of 0.24 °C/h, where water was used as a solvent. The structure of KLAM was solved by single-crystal XRD. KLAM crystallizes in $P2_1$ space group with unit cell parameters $a = 7.030(5)$Å, $b = 8.811(5)$ Å, $c = 7.638(5)$Å and $\beta = 114.891(5)°$. The crystal grows with bulky morphology in all three directions having (100), (1 0 0), (1 1 0), (0 1 1), (0 1 1), (001) and (00 1) prominent faces. Thermo-gravimetric analysis and Differential scanning calorimetry measurements show that KLAM is stable up to 80 °C. The crystal offers good optical transparency with a lower cut off as low as 297 nm. Second harmonic conversion efficiency measured on powder sample is 3.5 times that of potassium dihydrogen phosphate. Phase matching (PM) is observed on the *a*-plate of the KLAM. Noncollinear phase matching rings are also observed near the PM directions, which help to identify the PM directions. The observation of noncollinear second-harmonic rings up to third-order indicates high magnitudes of nonlinear optical coefficients. Single-pulse laser damage threshold value of the crystal is 3.07 GW/cm^2 at 1064 nm on the *a*-plate of the crystal.

1 Introduction

Nonlinear optical crystals play a key role in solid-state lasers [1–4], which generate light at varying frequencies through nonlinear optical processes [5–14]. Due to their versatile applications in scientific and technological fields, they have received extensive research interest. Nonlinear optical molecular crystals have advantages of low cost, chemical stability, large second harmonic coefficients, moderate birefringence ($\Delta n \sim 0.05 - 0.10$), wide transparency window with high transmission and high laser damage threshold all of which are of scientific and technological interest [15–28]. Saccharides (sugars) are organic materials composed of carbon, hydrogen and oxygen. The saccharides are chiral and crystallize in non-centrosymmetric crystal structure which is a prerequisite for the generation of second harmonic [5]. L-ascorbic acid, a water-soluble monosaccharide, forms bulky colourless crystals because of multi-directional hydrogen bonds [29]. Crystals which include water molecules in their structure, lose crystallinity when water goes out. Saccharide crystals possess second harmonic generation (SHG) capability and are potential material for phase matching [30]. Previous reports on lithium L-ascorbate dihydrate, D-isoascorbic acid, and lithium D-isoascorbate monohydrate have shown that saccharides possess moderate to large birefringence and low walk off angle of second harmonic light and therefore are easily phase-matchable [31–34]. Ascorbic acid is not very stable in solution as it oxidizes into dehydroascorbic acid on exposure to air, light, and elevated temperatures. Dehydroascorbic acid may further be converted to various degradation products, such as 2-furoic acid, 3-hydroxy-2-pyrone, furfural etc. [35–37]. However, they are quite stable in the crystalline state. A previous report on lithium salt of ascorbic acid shows that lithium ion's introduction improves its chemical and physical properties. Besides, crystal structure is modified, leading to the enhancement of nonlinear optical properties like conversion efficiency, laser damage threshold, and stability [33].

Supplementary Information The online version contains supplementary material available at https://doi.org/10.1007/s00340-020-07561-x.

✉ Dhanpal Bairwa
dhanpal@iisc.ac.in

[1] Department of Physics, Indian Institute of Science, Bangalore 560012, India

[2] PES University, Bangalore 560085, India

[3] Solid State and Structural Chemistry Unit, Indian Institute of Science, Bangalore 560012, India

For investigating the effect of other alkali metals such as potassium, we synthesized the potassium salt of L-ascorbic acid. It crystallizes as monohydrate, with $P2_1$ space group which satisfies the structural requirement of noncentrosymmetry for second-harmonic generation.

This paper discusses the synthesis, crystal growth, structural and thermal properties of potassium L-ascorbate monohydrate KLAM. Also, powder second harmonic generation by Kurtz Perry method, noncollinear and collinear phase matching and laser damage are investigated.

2 Experimental section

KLAM was synthesized by mixing L-ascorbic acid (4 N, Sigma Aldrich) and potassium carbonate (4 N, Sigma Aldrich) in stoichiometric ratio (2:1) in distilled water at room temperature. L-ascorbic acid reacts with potassium carbonate quickly with the evolution of CO_2. The chemical reaction is given below.

$$2C_6H_8O_6 + K_2CO_3 + H_2O \rightarrow 2\,KC_6H_7O_6.H_2O + CO_2 \uparrow .$$

The solution is stirred using a magnetic stirrer until all the CO_2 escapes. Since photochemical decomposition causes colour change from clear to yellowish-red, the solution was shielded from light exposure [38].

Before growing the crystal, the compound was recrystallized twice to increase purity. Crystals up to $55 \times 30 \times 15$ mm^3 were grown without seeding in about four weeks. Solution growth technique using modified Holden's rotary crystallizer yields full morphology and hence employed for this work. It was observed that the material's solubility increases with temperature, so crystals were grown by lowering the temperature in the range of 33–28 °C. As the solution was sensitive to temperature, the saturated solution's upper limit was kept at 33 °C. Seed crystals were first obtained by slow evaporation of water. Thus, a good seed crystal was introduced in the saturated solution, which was cooled at 0.01 °C/h rate using Eurotherm 2416 temperature controller. After about 20 days, crystals of size $35 \times 35 \times 20$ mm^3 in size were obtained. The photographs of as-grown crystals are shown in Fig. 1.

Single crystal X-ray diffraction experiment (SCXRD) was performed using Oxford Xcalibur diffractometer with Eos detector and Mova microscope ($\lambda = 0.71073$ Å). Direct method in Shelx 2014 was applied to solve the structure. To check the bulk purity and presence of a single phase in the entire crystal, powder X-ray diffraction was carried on Rigaku SmartLab X-ray diffractometer which employs Cu-K_α radiation. A contact goniometer (least count 0.1°) was used to measure the interfacial angles. Thermogravimetric analysis (TGA) was made with the help of

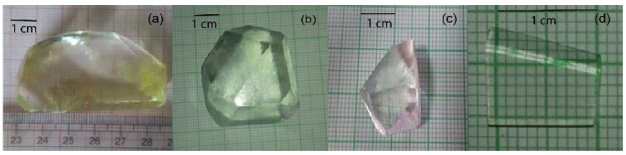

Fig. 1 **a** A KLAM crystal grown by slow evaporation without seeding. **b** and **c** crystals grown with solution growth set up by seeding. **d** polished plate cut perpendicular to **b** crystallographic axis

ME-51140728 model of ARTESYN technologies while Differential scanning calorimetry (DSC) experiments were carried out with the help of DSC 2920 model of TA Instruments. The UV–Vis transmission spectrum was recorded using UV-3600 spectrometer. For phase matching, laser damage and UV–Vis spectroscopy, polished (using methanol and Al_2O_3 powder) crystal plates were used. Crystals were cut using a homemade wet-saw machine, which cuts the crystal by dissolving the crystal by a fine wet string. For polishing, the crystal plates were rubbed on the BUEHLER's polishing micro cloth with methanol and alumina (Al_2O_3) powder of different particle sizes (3–0.5 µm). An Nd:YAG laser (1064 nm, 10 Hz repetition rate, 6 nm pulse width) was used for collinear and noncollinear phase matching. For laser damage studies, Nd:YAG and He–Ne lasers were used simultaneously as pump and probe. The energy of Nd:YAG and He–Ne lasers were measured using pyroelectric sensors PE25BBDIFSHV2 (with and without diffuser) and 3APSHV1, respectively, together with a NOVA II Ophir power meter. For visual verification of the damage, a Leitz Orthoplan microscope was used. For finding the relationship between crystallographic **a**, **b**, **c** directions and the direction of optical importance, Laue XRD was carried out using Rigaku diffractometer with Mo-K_α radiation (polychromatic). Optical measurements were carried out by keeping the crystal on a goniometer. The goniometer with the crystal was then transferred to the X-ray machine gently not to disturb the crystal from its position. Data were fitted using Orient express software.

3 Results and discussion

3.1 Single-crystal XRD

Crystallographic information obtained from SCXRD and details of data refinement are given in Table 1. KLAM crystallizes in monoclinic $P2_1$ space group at room temperature. Molecular diagram of KLAM is shown in Fig. 2. Along the **b** direction, potassium atoms are connected via O3 and O7W atoms. In **a** and **c** directions, they are connected through organic links as shown in the packing diagram of KLAM in

Table 1 Crystallographic data of KLAM obtained from SCXRD

Formula	$C_6H_9O_7K$
CCDC No	1944136
Formula weight	232.23
Temperature (K)	295 K
Colour	Colourless
Crystal size (mm^3)	$0.2\times0.15\times0.12$
Radiation	Mo-K_α
Wavelength (Å)	0.71073
Crystal system	Monoclinic
Space group	$P2_1$
a (Å)	7.030(5)
b (Å)	8.811(5)
c (Å)	7.638(5)
β (°)	114.891(5)
Volume ($Å^3$)	429.2(5)
Z	2
No. unique reflections	1660
No. of parameters	164
Theta min. and Theta max	3.741° and 30.061°
$R[F^2>2\sigma(F^2)]$, $wR_2(F^2)$	0.0451, 0.0977
$\Delta\rho_{min}$, $\Delta\rho_{max}$ ($eÅ^{-3}$)	−0.296, 0.365
Goodness of fit	1.013

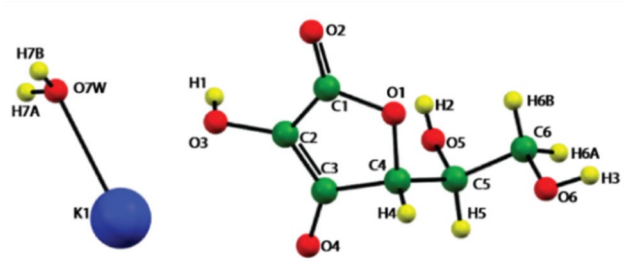

Fig. 2 Molecular diagram of potassium L-ascorbate monohydrate

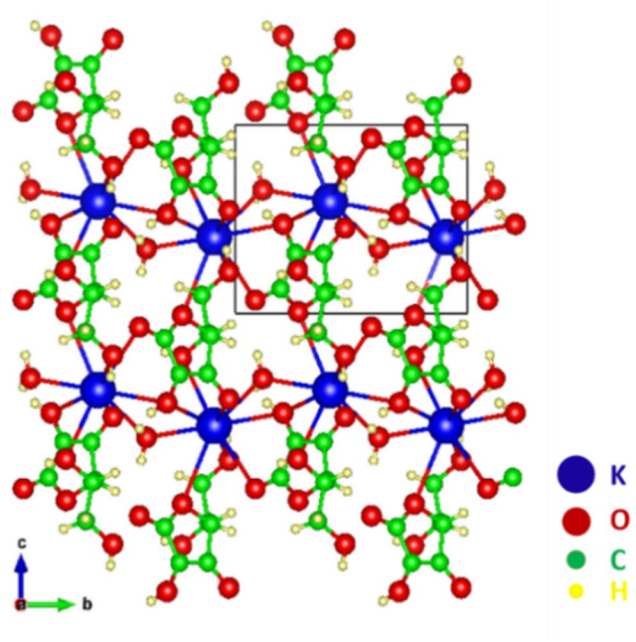

Fig. 3 Packing diagram of potassium L-ascorbate monohydrate perpendicular to **a** direction (double bonds are not shown for simplicity)

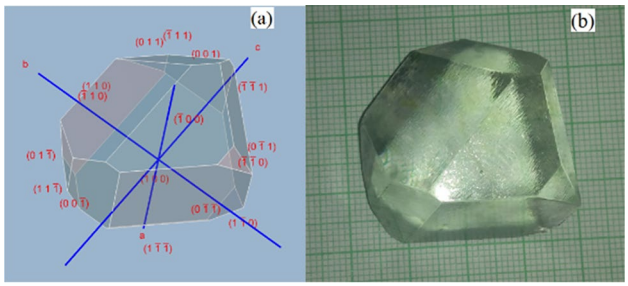

Fig. 4 **a** Morphology of the KLAM crystal generated by the Orient Express software which matches with the morphology of the crystal in (**b**)

Fig. 3. Hydrogen bonding figure and list of Hydrogen bonds are given in Figure S5 and Table S4, respectively.

3.2 Morphology

WinXmorph software was used to identify the morphology of the crystal [39, 40]. Given crystallographic data, the software generates morphology according to point group symmetry. Appropriate hkl values and central distances generate a figure identical to the crystal's morphology. Angles between the planes calculated from the software and those measured experimentally using a contact goniometer are listed in table S5. Theoretical and experimentally measured inter-planar angles show a good match. The morphology of the crystal generated is illustrated in Fig. 4a which looks similar to the grown crystal in 4(b). The crystal is bulky with 15 habit faces, though fewer faces develop (~12 number) in smaller crystals.

3.3 Thermal analysis

DSC and TGA curves for KLAM are shown in Fig. 5. Both measurements were performed at 5 °C/min heating rate. TGA curve shows that the material starts to lose weight from 80 °C. From 80 to 105 °C degree, it loses ~ 0.2121 mg weight, which is 5.81% of its initial weight of 3.65 mg. The theoretically calculated percentage of water is 7.751%. This is close to the experimentally measured value and indicates that KLAM loses most of the water between 80 and 105 °C. The range may vary with different heating rates. Beyond

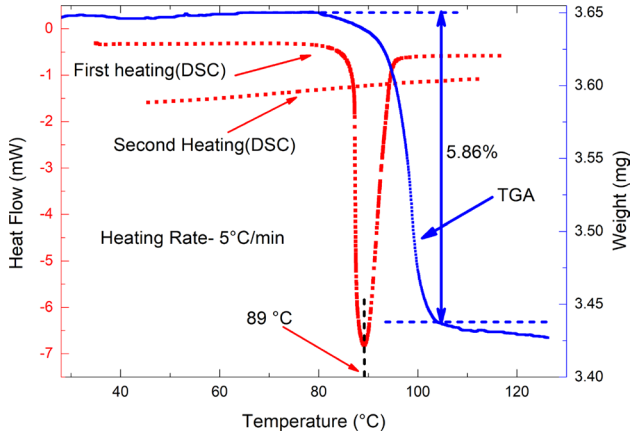

Fig. 5 TGA and DSC plots of KLAM. Note that the peak at 89 °C in the first DSC curve matches the onset of the weight loss in the TGA curve

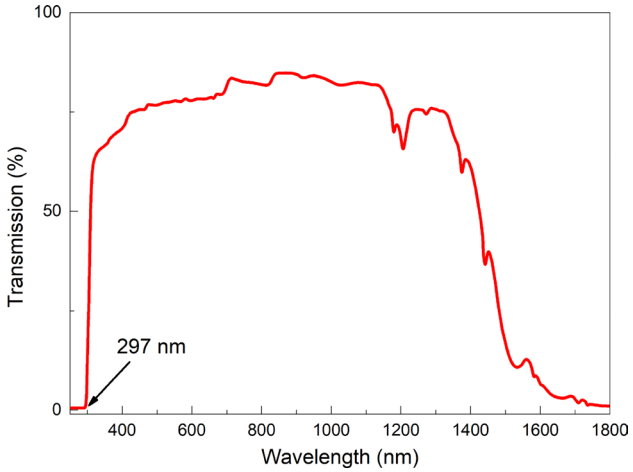

Fig. 6 Spectrum of UV–Vis transmission of KLAM crystal measured at a polished *a*-plate

105 °C, all remaining water goes out of the sample. At higher temperatures, weight loss could not be measured, as the material becomes foamy and bubbles out of the crucible. An endothermic peak at 89 °C in the DSC curve is attributed to dissociation of water molecules from the KLAM and subsequent evaporation of crystallized water, which is also in conformance with TGA data. During the second heating (of the same material), the endothermic peak was not observed, confirming that the endothermic peak is due to dissociation and evaporation of water molecule from KLAM. Results of both TGA and DSC endorse that KLAM is stable at least up to 80 °C which is the onset temperature in DSC. After this temperature, it loses crystallinity.

3.4 UV–Vis spectroscopy

Figure 6 shows the optical transmission spectrum of KLAM. A polished 1 mm thick *a*-plate was used. The graph shows that the crystal has more than 80% transparency in visible and good transmission in UV regions.

After 320 nm, transmission drops sharply and crystal becomes opaque at lower wavelengths. The lower cut off wavelength is 297 nm and the higher cut off is near 1500 nm, which indicates that crystal can be used in nonlinear optics for SHG and THG in visible and UV region. Calculated value of the bandgap from the lower cut off is 4.18 eV.

3.5 Powder SHG measurements

Since KLAM crystallizes in the non-centrosymmetric space group, it is expected to be NLO-active. We carried out SHG measurements using the Kurtz – Perry method [41]. Here Nd:YAG laser beam of 1064 nm wavelength with 10 ns pulse duration and 10 Hz repetition rate was used.

Fine powder of the crystal was packed tightly in a capillary tube. Focused laser beam of 1064 nm was made to fall on the tube and generated second harmonic. SHG signal was separated using a monochromator and was subsequently amplified by a photomultiplier tube and then measured by oscilloscope. SHG signal of the standard KDP powder was also measured in the same way. The intensities ratio shows that the second harmonic conversion efficiency of KLAM is 3.5 times that of KDP.

3.6 Collinear and Spontaneous noncollinear phase matching

Spontaneous noncollinear phase matching (SNCPM) is often observed in crystals with large birefringence and large NLO coefficients [32, 42]. NCPM arises due to the interaction of the fundamental beam with scattered light inside the crystal. When fundamental beam with wave vector $k_1(\lambda)$ falls on the crystal, most of it passes through the crystal unaltered but a small amount of the beam is scattered from the crystal surface and crystal imperfections, yielding the wave vector $k_1'(\lambda)$. If the wave vector for the second harmonic wave is $k_2(2\lambda)$, where the phase-matching condition $\Delta k = (k_2 - 2k_1) = 0$ is satisfied, second harmonic light is amplified [42].

To observe SNCPM and collinear phase matching (CPM), *a*-plate of KLAM crystal was oriented such that crystallographic [100] direction was along the OX axis and [010] direction along the OZ axis of the goniometer. The corresponding Laue pattern (experimental and computed) for this orientation is shown in Figure.S3. The positive directions of rotation of the goniometer axes are also shown in Fig. 7.

The crystal was then rotated around [010] direction, during which SNCPM rings were initially observed. On further

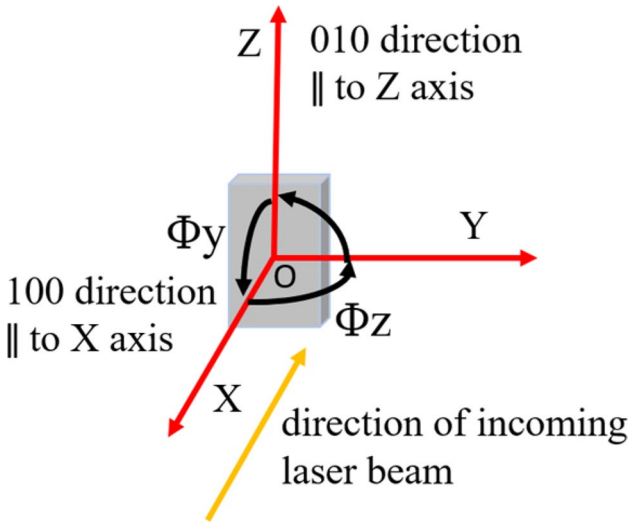

Fig. 7 Crystallographic and incoming laser beam direction with respect to goniometer axis. Arrows in black colour show the positive direction of rotation

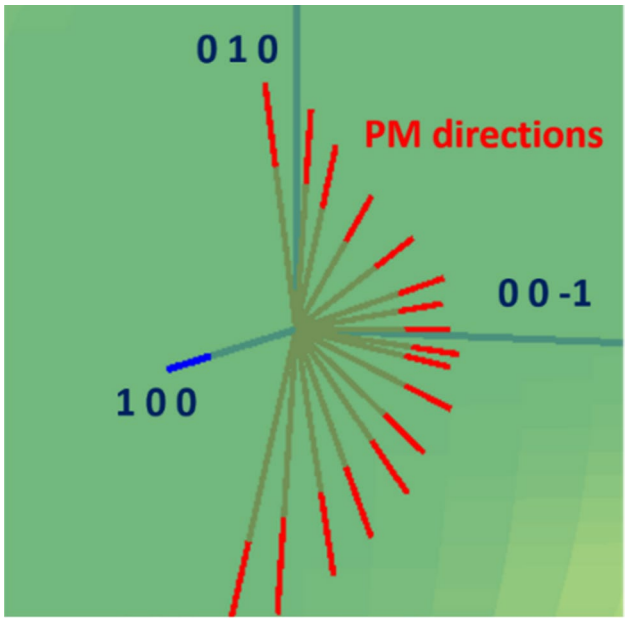

Fig. 9 Experimentally measured phase-matching directions in KLAM

rotating the crystal anticlockwise, collinear phase matching was observed at 13.5°, the evolution of which is shown in Fig. 8. On further rotation from CPM direction by small angle (~2°), the SHG signal intensity drastically reduces. Thus, SNCPM has helped us in identifying a phase-matching direction.

To measure the other phase-matching directions experimentally, rotation around OY direction was employed with the rotation around OZ axis. List and plot (Matlab) of angles at which phase matching was obtained by varying ϕy and ϕz are shown in table S6 and Fig. 9, respectively.

3.7 Laser damage studies

To resist the high laser power density for a crystal is a crucial factor in nonlinear optics. In laser damage studies, single pulse and multiple pulse threshold values are important. The highest power density up to which the crystal surface remains intact is defined as the damage threshold. For single pulse damage, a fresh surface was exposed to avoid history effect. Single and multiple pulse damage threshold values of KLAM crystal were measured using Nd:YAG laser in TEM_{00} mode with a pulse width of 6 ns and 10 Hz repetition rate. Multiple pulse damage studies were carried out by employing the procedure defined by Nakatani [43]. The threshold value is always lower for multiple pulses than the single pulse due to the collective effect [44]. A plano-convex lens of 30 cm focal length was used at beam waist to focus the laser beam on the crystal surface.

With M^2 value equal to 2, 1064 nm wavelength and 6 mm beam waist, the focused spot diameter was calculated to be 135 µm using the relation.

$$d' = 4M^2\lambda f/\pi d.$$

The damage was inspected continuously by measuring the He–Ne laser intensity, passing through the crystal collinearly with the Nd:YAG laser beam. The occurrence of damage causes an abrupt decrease in the intensity of He–Ne laser. Further verification of the damage was done by examining the crystal under a Leitz orthoplan microscope.

A polished *a*-plate of the KLAM crystal was used for damage studies. Figure 10 shows the plot of damage threshold (average) with the number of pulses impinging

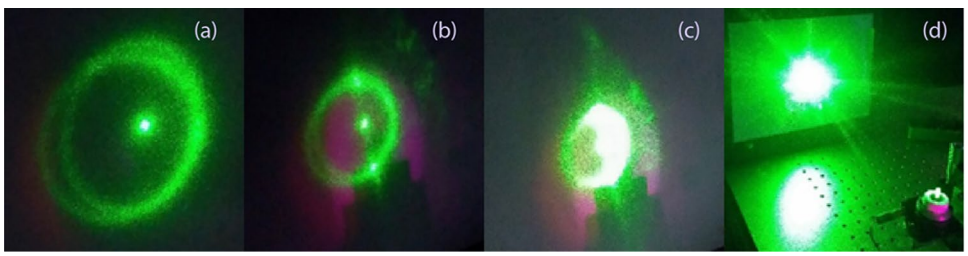

Fig. 8 Evolution of SNCPM rings into collinear PM spot in the *a*-plate of KLAM crystal

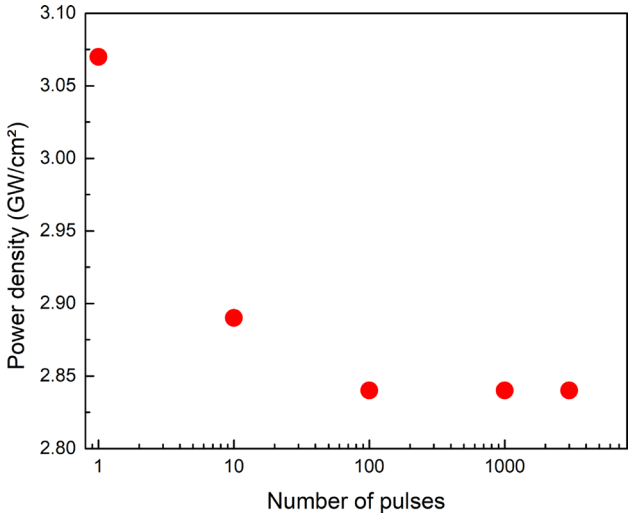

Fig. 10 Plot of damage threshold (average) with the number of pulses irradiated on the crystal surface

on the crystal surface. The average damage threshold value for a single pulse is 3.07 GW/cm^2 and for multiple pulses (3000 pulses) is 2.84 GW/cm^2. The reason for the damage is identified as dielectric breakdown as for short pulses (10^{-8}–10^{-10} ns pulse width); this is generally the most prominent reason [45]. There was no sign of melting after the damage which supports this view. Nearly 70% of the damage was observed on the exit surface of the crystal. Boling and Crisp brought forward an explanation for the damage at exit surface [46].

4 Conclusion

Large size crystals of KLAM were successfully grown by solution growth technique. Single-crystal XRD reveals that KLAM crystallizes in the monoclinic $P2_1$ space group. The crystal possesses bulky morphology and is stable up to 80 °C after which it loses water and hence crystallinity. SHG conversion efficiency of this material is 3.5 times that of KDP, as revealed by powder Kurtz Perry technique. In noncollinear phase matching, rings up to third order were observed which indicate high conversion efficiency. Noncollinear phase matching was observed on *c*-plate [Figure S4]. Both collinear phase matching and noncollinear phase matchings were experimentally observed on the *a*-plate of the crystal. Single-pulse laser damage threshold value observed on *a*-plate is 3.07 GW/cm^2. Good SHG conversion efficiency, collinear and spontaneous noncollinear phase matching ability make this material potentially useful for nonlinear optical applications.

Acknowledgements The authors are grateful to Prof. P.K. Das, IISc, Bangalore for the measurement of SHG efficiency by Kurtz-Perry method. The authors acknowledge the support of the departmental central facility funded by the University Grants Commission.

References

1. T. Taira, T. Kobayashi, Q-switched and frequency doubling of solid-state lasers by a single intracavity KTP crystal. IEEE J. Quantum Electron. **30**, 800–804 (1994)
2. G.A. Rines, H.H. Zenzie, R.A. Schwartz, Y. Isyanova, P.F. Moulton, Nonlinear conversion of Ti:sapphire lasers. IEEE J. Select. Topics Quantum Electron. **1**, 50–57 (1995)
3. P.V. Kolinsky, New materials and their characterization for photonic device. Opt. Eng. **31**, 1676–1684 (1992)
4. H.S. Nalwa, Organometallic materials for nonlinear optics. App. Organomet. Chem. **5**, 349–377 (1991)
5. P.A. Franken, J.F. Ward, Optical harmonics and nonlinear phenomena. Rev. Mod. Phys. **35**, 23–39 (1963)
6. P.A. Franken, A.E. Hill, C.W. Peters, G. Weinreich, Generation of optical harmonics. Phys. Rev. Lett. **7**, 118–120 (1961)
7. A. Giordmaine, Mixing of light beams in crystals. Phys. Rev. Lett. **8**, 19–21 (1962)
8. C.C. Wang, G.W. Racette, Measurement of parametric gain accompanying optical difference frequency generation. Appl. Phys. Lett. **6**, 169–171 (1965)
9. J.E. Bjorkholm, Optical second-harmonic generation using a focused gaussian laser beam. Phys. Rev. **142**, 126–136 (1966)
10. N. Bloembergen, P.S. Pershan, Light waves at the boundary of nonlinear media. Phys. Rev. **128**, 606–622 (1962)
11. J.A. Giordmaine, R.C. Miller, Tunable coherent parametric oscillation in $LiNbO_3$ at optical frequencies. Phys. Rev. Lett. **14**, 973–976 (1965)
12. J.F. Ward, P.A. Franken, Structure of nonlinear optical phenomena in potassium dihydrogen. Phosphate Phys. Rev. **133**, A183–A190 (1964)
13. Y.R. Shen, *The Principles of Nonlinear Optics* (Wiley, New York, 1984).
14. R.W. Boyd, *Nonlinear Optics* (Academic, Boston, 1992).
15. Y.N. Xia, C.T. Chen, D.Y. Tang, B.C. Wu, New nonlinear optical crystals for UV and VUV harmonic generation. Adv. Mater. **7**, 79–81 (1995)
16. L. Kang, S.Y. Luo, H.W. Huang, N. Ye, Z.S. Lin, J.G. Qin, C.T. Chen, Prospects for fluoride carbonate nonlinear optical crystals in the UV and deep-UV regions. J. Phy. Chem. C. **117**, 25684–25692 (2013)
17. T.T. Tran, H.W. Yu, J.M. Rondinelli, K.R. Poeppelmeier, P.S. Halasyamani, Deep ultraviolet nonlinear optical materials. Chem. Mater. **28**, 5238–5258 (2016)
18. Y. Wang, B.B. Zhang, Z.H. Yang, S.L. Pan, Cation-tuned synthesis of fluorooxoborates: towards optimal deepultraviolet nonlinear optical materials. Angew. Chem. Int. Ed. **57**, 2150–2154 (2018)
19. M. Gryl, T. Seidler, J. Wojnarska, K. Stadnicka, I. Matulkova, I. Nemec, P. Nemec, Co-crystals of 2-amino-5-nitropyridine barbital with extreme birefringence and large second harmonic generation effect. Chem. Eur. J. **24**, 8727–8731 (2018)
20. W. Zhu, L. Zhu, L. Sun, Y. Zhen, H. Dong, Z. Wei, W. Hu, Uncovering the intramolecular emission and tuning the nonlinear optical properties of organic materials by cocrystallization. Angew. Chem. Int. Ed. **55**, 14023–14027 (2016)
21. P. Karuppasamy, M. Senthil Pandian, P. Ramasamy, S.K. Das, Growth and characterization of semi organic nonlinear optical (NLO) guanidinium trichloroacetate (GTCA) single crystal. Optik **156**, 707–719 (2018)

22. B.L. Wu, C.L. Hu, F.F. Mao, R.L. Tang, J.G. Mao, Highly polarizable Hg^{2+} induced a strong second harmonic generation signal and large birefringence in $LiHgPO_4$. J. Am. Chem. Soc. **141**, 10188–10192 (2019)
23. T.W. Kasel, Z. Deng, A.M. Mroz, C.H. Hendon, K.T. Butler, P. Canepa, Metal-free perovskites for nonlinear optical materials. Chem. Sci. **10**, 8187–8194 (2019)
24. T. Pei, L. Zhou, Q. Zhang, D. Ma, Y. Bai, Q. Yin, C. Xie, Studies on structure, NLO properties of a new organic NLO crystal: guanidinium 3,5-dihydroxybenzoate. J. Mater. Sci. **30**, 2994–3003 (2019)
25. H. Yu, N.Z. Koocher, J.M. Rondinelli, P.S. Halasyamani, Pb2BO3I: a borate iodide with the largest Second-Harmonic Generation (SHG) response in the KBe2BO3F2 (KBBF) family of Nonlinear Optical (NLO) Materials. Angew. Chem. Int. Ed. **57**, 6100–6103 (2018)
26. Y. Li, F. Liang, S. Zhao, L. Li, Wu. Zhenyue, Q. Ding, S. Liu, Z. Lin, M. Hong, C.J. Luo, Two non-π-conjugated deep-UV nonlinear optical sulfates. J. Am. Chem. Soc. **141**(9), 3833–3837 (2019)
27. S. Zhao, X. Yang, Yi. Yang, X. Kuang, Lu. Fengqi, P. Shan, Z. Sun, Z. Lin, M. Hong, J. Luo, Non-centrosymmetric $RbNaMgP_2O_7$ with unprecedented thermo-induced enhancement of second harmonic generation. J. Am. Chem. Soc. **140**(5), 1592–1595 (2018)
28. Y. Liu, Y. Shen, S. Zhao, J. Luo, Structure-property relationship in nonlinear optical materials with π-conjugated CO_3 triangles. Coord. Chem. Rev. **407**, 213152 (2020)
29. J. Hvoslef, The crystal structure of L-ascorbic acid, `vitamin C'. II. The neutron diffraction analysis. Acta Cryst. **B24**, 1431–1440 (1968)
30. G. Bourhill, K. Mansour, K.J. Perry, L. Khundkar, E.T. Sleva, R. Kern, J.W. Perry, I.D. Williams, S.K. Kurtz, Powder second harmonic generation efficiencies of saccharide materials. Chem. Mater. **5**, 802–808 (1993)
31. K.R. Rao, C. Aneesh, H.L. Bhat, S. Elizabeth, M.S. Pavan, T.N. Guru Row, Lithium D-isoascorbate monohydrate, a new nonlinear optical material. Cryst. Growth Des. **13**, 97–105 (2013)
32. K.R. Rao, H.L. Bhat, S. Elizabeth, Crystal growth and nonlinear optical properties of sodium D-isoascorbate monohydrate. CrystEngComm **15**, 6594–6601 (2013)
33. K.R. Rao, H.L. Bhat, S. Elizabeth, Studies on lithium L-ascorbate dihydrate: an interesting chiral nonlinear optical crystal. Mater. Chem. Phys. **137**, 756–763 (2013)
34. K.R. Rao, R. Sanathkumar, H.L. Bhat, S. Elizabeth, The nonlinear optical properties of the monoclinic D-isoascorbic acid crystal. Appl. Phys. B **122**, 270 (2016)
35. E. Kimoto, H. Tanaka, T. Ohmoto, M. Choami, Analysis of the transformation products of dehydro-L-ascorbic acid by ion-pairing high-performance liquid chromatography. Anal. Biochem. **214**, 38–44 (1993)
36. J.-P. Yuan, F. Chen, Degradation of ascorbic acid in aqueous solution. J. Agric. Food Chem. **46**, 5078–5082 (1998)
37. Kuellmer V (2001) Ascorbic acid. In: Kirk-Othmer encyclopedia of chemical technology. Wiley, New Jersey. https://doi.org/10.1002/0471238961.0119031511210512.a01.pub2
38. A.E. Kellie, S.S. Zilva, The photochemical decomposition of L-ascorbic acid. Biochem. J. **32**, 1561–1565 (1938)
39. W. Kaminsky, WinXMorph: a computer program to draw crystal morphology, growth sectors and cross sections with export files in VRML V2.0 utf8-virtual reality format, J. Appl. Crystallogr. 38, 566–567 (2005). Available at http://cad4.cpac.washington.edu/WinXMorphHome/WinXMorph.htm.
40. W.J. Kaminsky, From CIF to virtual morphology using the WinXMorph program. J. Appl. Cryst. **40**, 382–385 (2007)
41. S.K. Kurtz, T.T. Perry, A powder technique for the evaluation of nonlinear optical materials. J. Appl. Phys. **39**, 3798–3813 (1968)
42. J.A. Girdmaine, Mixing of light beams in crystals. Phs. Rev. Lett. **8**, 19–21 (1962)
43. H. Nakatani, W.R. Bosenberg, L.K. Cheng, C.L. Tang, Laser-induced damage in beta-barium metaborate. Appl. Phys. Lett. **53**, 2587–2589 (1988)
44. V. Venkataraman, C.K. Subramanian, H.L. Bhat, Laser induced damage in zinc tris(thiourea) sulphate and bis(thiourea) cadmium chloride. J. Appl. Phys. **77**, 6049–6051 (1995)
45. R.M. Wood, *Laser-Induced Damage of Optical Materials* (CRC Press, Boca Raton, 2003).
46. N.L. Boling, M.D. Crisp, G. Dube, Laser induced surface damage. Appl. Opt. **12**, 650–660 (1973)

Publisher's Note Springer Nature remains neutral with regard to jurisdictional claims in published maps and institutional affiliations.